Modulating Conductivity, Environmental Stability of Transparent Conducting Nanotube Films on Flexible Substrates by Interfacial Engineering

Joong Tark Han, Jun Suk Kim, Hae Deuk Jeong, Hee Jin Jeong, Seung Yol Jeong, and Geon-Woong Lee*

Nano Carbon Materials Research Group, Korea Electrotechnology Research Institute, Changwon, 641-120 Korea

ABSTRACT We have characterized the previously undescribed parameters for engineering the electrical properties of single-walled carbon nanotube (SWCNT) films for technological applications. First, the interfacial tension between bare SWCNT network films and a top coating passivation material was shown to dictate the variability of the films' sheet resistance (R_s) after application of the top coating. Second, the electrical stability of the coated SWCNT films was affected by the mismatch between the CTE of the supporting substrate and the SWCNT network film. An upshift in the Raman G-band spectrum of SWCNTs on bare PET suggested that compressive strain was induced by the CTE mismatch after heating and cooling. These findings provide important guidelines for the choice of substrate and passivation coating materials that promote environmental stability in SWCNT-based transparent conductive films.

KEYWORDS: single-walled carbon nanotubes · surface tension · thermal expansion coefficient mismatch · top coating · silane sol

Single-walled carbon nanotube (SWCNT) network films have been intensively studied for the development of alternative transparent conductive electrodes due to the excellent electrical properties and flexibility of SWCNT networks and their solution processability under ambient conditions.[1−9] The conductivity of SWCNT films depends on several intrinsic and extrinsic properties of the nanotubes, including purity, the volume fraction of metallic *versus* semiconducting nanotubes, and the doping level of the semiconducting tubes.[10−14] In addition, the geometry of the bundles that form the network substantially influences the network conductivity.[15−18] The conductivity of SWCNT films may be manipulated by acid treatment of surfactant-assisted SWCNT films.[19] Electrode applications in devices such as touch panels, organic light-emitting diodes, solar cells, and displays require passivation of the SWCNT films by a top coating process using organic or inorganic materials that inhibit nanotube oxidation or adsorption of water molecules when the network is exposed to high temperatures or humidity. Passivation by a top coating significantly improves the environmental stability of the films.[20−23] However, the importance of the wetting properties of top coating materials was not recognized. Control of these properties is crucial for minimizing the sheet resistance increased by the top coating with an insulating material. The interfacial tension between the SWCNT network and the top coating material can influence the porosity of the film, the packing density of the carbon nanotubes (CNTs), and the junction resistance across SWCNT bundles, which are important parameters for the DC conductivity of the SWCNT films.[15]

The stability of the conductivity of SWCNT network films at high temperatures, beyond 100 °C, is an important property of SWCNT films on flexible substrates for electrode applications because electrodes may be exposed to high temperatures during the assembly process. Therefore, the thermal expansion of the substrate has to be compatible with that of the SWCNT network film. Deformation of SWCNT networks occurs after heating and cooling processes if the coefficients of thermal expansion (CTE) for the SWCNT network film and the flexible substrate are not matched. Previous reports showed that mismatch between the CTE of the matrix and CNT network in CNT/polymer composites induced thermal residual radial stress and deformation along the nanotubes when the polymer was cooled from its melt.[24,25] Deformation of the SWCNTs that interacted with the substrate affected the intrinsic conductivity of the SWCNT network or the junction resistance of the network film.[26−31]

*Address correspondence to gwleephd@keri.re.kr.

Received for review March 31, 2010 and accepted July 14, 2010.

Published online July 22, 2010.
10.1021/nn100650e

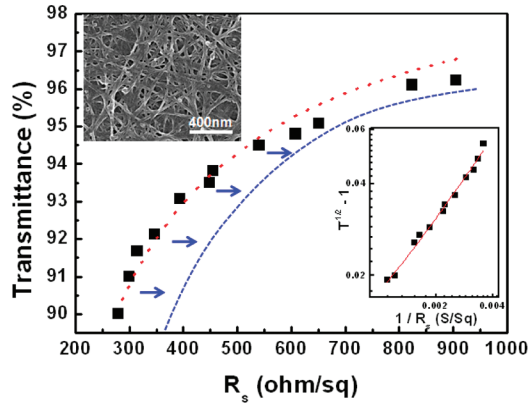

Figure 1. Transmittance (550 nm) as a function of sheet resistance for bare SWCNT thin films. The inset shows a scanning electron microscopy (SEM) image of a bare SWCNT film. The dotted red line was fit to eq 1, consistent with a σ_{DC}/σ_{Op} value of 12.7. Inset plot: Transmittance *versus* sheet resistance data plotted to emphasize the goodness of fit to eq 1. The inset shows a typical SEM image of a bare SWCNT film.

Therefore, elucidating the effect of the interfacial tension between SWCNTs and top coating materials, and the CTE mismatch between SWCNTs and their substrates on the conductivity of the SWCNT network film, are critical for the success of applications. Until now, these parameters have not been intensively considered with respect to enhancing the performance and thermal stability of SWCNT-based TCFs on flexible substrates.

Here, we describe several factors that are keys to the fabrication of highly conductive thermally stable SWCNT films on flexible substrates. Notably, this study suggests that controlling the interfacial tension between the SWCNT network films and the top coating material permits tuning of the electrical conductivity of SWCNT films. Silane sols with varying surface tensions were used as the top coating material on SWCNT films. Moreover, it was found that the doping process not only controlled the electronic structure of the SWCNTs, but also manipulated the surface tension of the SWCNT surface. This study also demonstrated that the compressive strain of SWCNTs induced by the difference in CTE between SWCNTs and the flexible substrate with high thermal expansion behavior led to an increase in the sheet resistance after heating and cooling.

RESULTS AND DISCUSSION

Unusual Decrease in the Sheet Resistance of SWCNT Films by Application of a Top Coating. SWCNT films were prepared by air spraying from an aqueous dispersion of arc-SWCNTs (purchased from Nano Solutions, Korea) aided by sodium dodecylbenzenesulfonate on selected substrates: polyethylene terephthalate (PET), hard-coated PET, and glass treated with phenyltrimethoxysilane (PTMS) for effective adhesion of the SWCNTs. Figure 1 shows a plot of the sheet resistance (R_s) *versus* transmittance and a typical photograph of the SWCNT films on bare PET. The films had porous structures on the scale of tens of nanometers. SWCNT films with 90% transmittance and 274 Ω/sq sheet resistance were used for top coating tests. Sheet resistance and transmittance are related by[3]

$$T(\lambda) = \left(1 + \frac{188.5}{R_s}\frac{\sigma_{Op}(\lambda)}{\sigma_{DC}}\right)^{-2} \quad (1)$$

where σ_{DC} and σ_{Op} are the DC and optical conductivities, respectively.

Eq 1, combined with the values for R_s and T, implied a value of $\sigma_{DC}/\sigma_{Op} \approx 13$. This value was comparable to the best performance reported for pristine SWCNT network films, even though thermally treated arc-SWCNTs were used here.[32,33]

The conductivity, σ_{DC}, of the disordered nanotube films depends on the number density of the network junctions, N_j, which in turn scales with the network morphology though the film fill-factor, V_f, the mean diameter, $<D>$, of the bundles, and the mean junction resistance, $<R_J>$,[15−18]

$$\sigma_{DC} = \frac{K}{<R_J><D>^3}\frac{V_f^2}{} \quad (2)$$

Here, K is the proportionality factor that scales with the bundle length. Therefore, changes in $<R_J>$ and V_f *via* application of a top coating may be influenced by the wetting properties of the SWCNT films. Top coatings composed of insulating materials would be expected to increase the sheet resistance of the film due to increased probe contact resistance and junction resistance, as plotted in Figure 1 (dotted blue line). Importantly, the conductivity of the SWCNT network films depends significantly on the porosity of the film and the junction resistance. We therefore presumed that if the packing density of the porous SWCNT network were increased, and R_J were decreased by controlling the interfacial tension between nanotube bundles and top coating materials, then the conductivity of the film would increase. The magnitude of the interfacial tension is determined primarily by the disparity between the polarities of the two phases. The greater the polarity difference, the greater the interfacial tension.[34,35] Thus, to increase the surface energy of the SWCNT without introducing defect sites, $AuCl_3$ dissolved in ethanol was deposited on the pristine SWCNT films. After doping, the sheet resistance and transmittance of the film were measured to be 139 Ω/sq and 90%, respectively. These properties corresponded to a value of $\sigma_{DC}/\sigma_{Op} \approx 25$, which was similar to that reported previously.[33] The water contact angle of the film decreased from 106° to 49°, as shown in Figure 2A, implying that the high surface energy of the film was realized by Au doping.

Two top coating materials, a tetraorthosilicate (TEOS) sol with silanol groups and methyltrimethoxysi-

lane (MTMS) sol with hydrophobic methyl groups, were applied to the bare SWCNT films to control the interfacial tension. The sol solution (solid content 17 wt %) was prepared as described previously.[36] The dilution solvent was exchanged with DMF to remove water introduced initially to hydrolyze the silane precursor, which permits long-term storage. The diluted sol solution (0.2 wt % by solid content) was coated onto the bare SWCNT films by air spraying. The thickness of the top coating layer was controlled by the number of spray applications. When applied to Si wafers, the thickness increased linearly by 2 nm after each spray application. However, it was difficult to estimate the exact top coating layer thickness on SWCNT films because the silane sols filled the pore structures of the film. Figure 2B shows the sheet resistance of the SWCNT films as a function of the number of top coating spray applications. In the undoped system, the sheet resistance of the film top-coated with the MTMS sol gradually increased until saturation as the top coating layer thickness increased. The sheet resistance of the film coated with the TEOS sol unexpectedly decreased to less than 80% of the sheet resistance of the bare SWCNT film (R_s ~208 Ω/sq at 90% transparency), despite the insulating characteristics of SiO_2. These values corresponded to a $\sigma_{DC}/\sigma_{Op} \approx 16.6$. We note that these ratios were higher than the ratio of the best film produced to date without post treatment (such as acid treatment), even after application of an insulating top coating material. Moreover, this ratio was even larger than that ($\sigma_{DC}/\sigma_{Op} = 15$) of SWCNT/poly(3,4-ethylenedioxythiophene):poly(styrene sulfonate) composite films prepared by the vacuum filtration method.[37] The large disparity in sheet resistance values for the MTMS and TEOS sol top coatings decreased upon modification of the bare SWCNT films with dopant molecules (Au^+), as shown in Figure 2B. The sheet resistance of the doped SWCNT films, after 5 spray applications of the TEOS sol coating, increased, then slightly decreased after 40 coating applications. Moreover, the MTMS sol did not trigger the dramatic increase in R_s due to the increased surface tension of the doped SWCNT network film. These results implied that the wettability of the silane sol coating applied to the SWCNT surface influenced the network morphology.

The sheet resistance changes of the SWCNT film after successive applications of the top coating may be understood by considering the surface tension of the components (nanotubes and silane sols). Previously, Dujardin *et al.*[38,39] reported that the critical surface tension for CNTs fell within the interval 40−80 mN/m, and the cutoff value that corresponded to cos θ = zero, γ_{max}, fell within the interval 130−170 mN/m. Liquids with $\gamma < \gamma_C$ yielded complete wetting upon formation of a thin film. For $\gamma_C < \gamma < \gamma_{max}$, partial wetting of the liquid occurred. The liquid did not wet the surface for $\gamma > \gamma_{max}$. SWCNTs, therefore, may be wetted by most

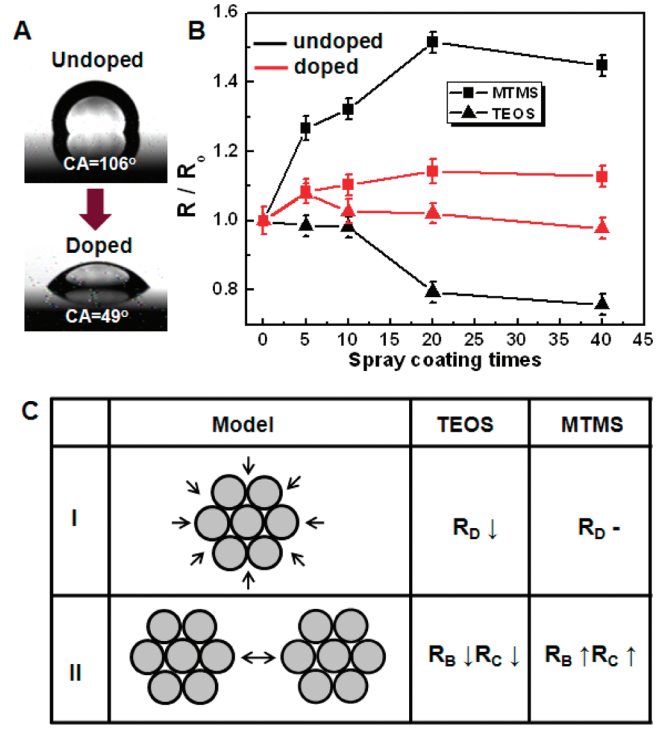

Figure 2. (A) Water contact angles on undoped SWCNT and doped SWCNT films. (B) Sheet resistance as a function of top coating times after baking at 80 °C for 1 h; black and red lines indicate the undoped and doped SWCNT films, respectively. (C) Cross-sectional view of the SWCNT bundles schematically shows the forces at work on the bundle after application of the top coating. (I): Model I, in which individual SWCNT bundles are affected by the top coating. (II): Model II, in which the interbundle distance is affected by the interfacial tension between the SWNCT surface and the top coating material.

polymer materials with surface tensions that fall in the interval 30−50 mN/m. Randomly oriented SWCNT network films include a large number of nanotube junctions. Such crossover sites attract polymeric materials *via* capillary effects.[39] On the other hand, the surface tension of the MTMS sol was less than 30 mN/m,[40] and that of the TEOS sol was around 170 mN/m.[41] Therefore, the MTMS sol was expected to easily wet the SWCNT surface and penetrate into the network junctions, whereas the TEOS sol, with its high surface tension, was expected not to wet or to only partially wet the nanotube surfaces. Figure 3 shows representative SEM images of the surfaces of top-coated SWCNT films. Undoped SWCNT bundles were found to be fully covered by the MTMS sol and partially covered by the TEOS sol, as indicated by the dotted line in Figure 3B. Furthermore, the network films coated with the TEOS sol were less porous than films coated with the MTMS sol, even after 5 spray applications. The porosity indicated that the MTMS sol fully coated the SWCNT bundles by van der Waals forces, thereby increasing the junction resistance, whereas the TEOS sol filled much of the network free volume (interstices) without penetrating the junctions. It is worth noting that the nonwetting properties of the TEOS sol may have resulted in densification of the SWCNT bundle network structure due to the geometri-

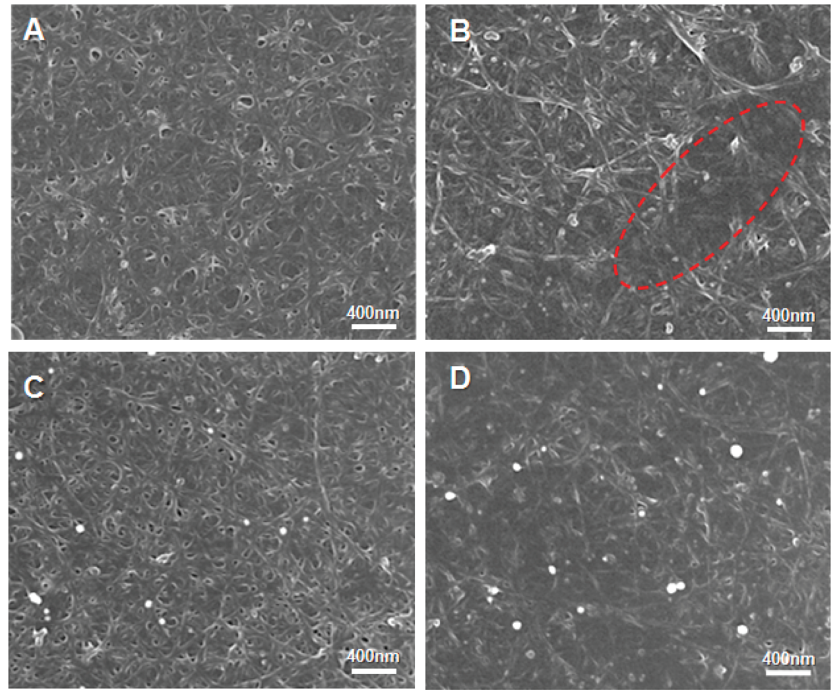

Figure 3. SEM images of (A and B) undoped SWCNT films and (C and D) doped SWCNT films after 5 spray applications of top coatings of (A and C) MTMS sol; (B and D) TEOS sol. The dotted circle in panel B indicates the TEOS sol-rich region.

cal constraints of the TEOS sol on the nanotube bundle surfaces. This, in turn, may have caused the unusual decrease in the sheet resistance. Doping with gold ions decreased the interfacial tension between nanotube bundles and the TEOS sol, whereas the interfacial tension between nanotube bundles and the MTMS sol increased. Formation of a complete TEOS sol coating in the doped system required only five spray applications due to the hydrophilic characteristic of the doped SWCNT film surface (Figure 3D). Dopants are usually used to control the electronic structure of semiconducting nanotubes. Our results demonstrated that dopants not only induced charge transfer, but also controlled the surface energy by minimizing the interfacial energy difference between nanotubes and top coating materials without damaging the nanotube structures.

R_J in eq 2 is composed of the contact resistance between the bundles R_C, the resistance network associated with charge transport across the bundle R_B, and the resistor network associated with transport across the full diameter of the bundle R_D. We suggest possible methods for varying R_J using top coatings with insulating materials, as shown in Figure 2C. A high interfacial tension between hydrophobic SWCNTs and hydrophilic TEOS sol may have decreased R_B, R_C, and R_D because the van der Waals forces between SWCNTs were much larger than the interaction forces between SWCNTs and the TEOS sol. On the other hand, the affinity of the MTMS sol for the hydrophobic SWCNT surface led to increases in R_B and R_C (model II), although R_D may not have been affected by the MTMS sol due to the strong van der Waals forces between individual SWCNTs (model I).

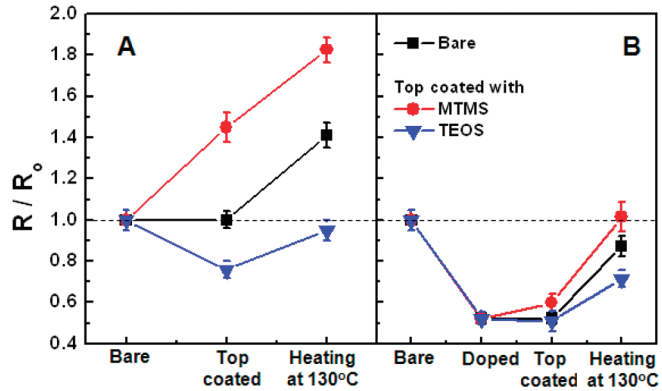

Figure 4. Sheet resistance changes of (A) undoped and (B) doped SWCNT films coated with silane sols after heating at 130 °C for 1 h.

Compressive Strain Induced an Increase in the Sheet Resistance. Recently, Ozel *et al.* reported that a disparity between the CTE of the substrate and the CTE of aligned SWCNTs grown by chemical vapor deposition on a single quartz crystal caused compressive stresses.[25] However, the importance of matching the CTEs of the SWCNTs and the substrate has not been recognized for TCF applications. The linear CTE is an order of magnitude smaller in SWCNTs ($(1-7) \times 10^{-6}\ K^{-1}$) than in thermoplastic polymers ($(1-10) \times 10^{-5}\ K^{-1}$).[42] Therefore, the CTE mismatch between nanotube networks and plastic substrates will be significant when the polymer substrate is cooled after heating, inducing substantial deformations in the SWCNT network that is in direct van der Waals contact with the polymer substrate and leading to variations in the electronic structure of SWCNTs. The strain can cause small gap openings in the elec-

tronic density of states in metallic SWCNTs under varying magnitudes of uniaxial strain.[31] Previous studies have shown that the electronic band gaps of semiconducting SWCNTs could be altered by mechanical stress.[29] The sign and magnitude of the band gap changes due to strain depend on the chiral angle.[29,43] Furthermore, Ni *et al.* recently reported that the band gap in graphene could be opened by applying uniaxial strain on graphene deposited on PET substrates.[44] Previous experimental and theoretical reports showed that the G-band phonon energy of SWCNTs increased under tensile strain or decreased under compressive strain, and this energy was sensitive to the electronic properties of SWCNTs.[43−48] Therefore, we presumed that the CTE mismatch between the SWCNT film and the substrate caused the increase in R_s after thermal stability tests at 130 °C.

The stability of film conductivity was estimated by fabricating SWCNT films on bare PET at 130 °C, followed by cooling over a period of 1 h. Interestingly, the sheet resistance of the bare SWCNTs and the MTMS-coated SWCNT films on PET substrates increased by 40% relative to the initial values, even in doped films, as shown in Figure 4. To illustrate this CTE mismatch effect, we compared the sheet resistance changes of SWCNT films fabricated on bare PET, hard-coated PET, and glass substrates, all of which displayed different thermal expansion properties. As shown in Figure 5, the sheet resistance increase was suppressed in bare SWCNT films on hard-coated PET and glass, which both presented small degrees of thermal expansion at 130 °C, relative to the sheet resistance increase of SWCNT films on bare PET. These results imply that the thermal stability of SWCNT-based films was enhanced through the use of flexible substrates coated with hard coating materials that were characterized by a small CTE. Moreover, the cured TEOS sol layer, with a high glass transition temperature (T_g), more effectively minimized the sheet resistance increase than did the MTMS sol, with a low T_g of <100 °C (Figure 4A).

The nature of the stress, tensile or compressive, experienced by SWCNTs on polymer substrates was investigated by comparing the Raman G-band frequencies of samples prepared on bare PET, hard-coated PET, and glass. The Raman spectrum at an excitation energy of 1.96 eV comprised a convolution of several peaks due to the presence of both semiconducting and metallic SWCNTs. Semiconducting tubes (s-SWCNT) show both G+ and G− peaks with Lorentzian shapes. Metallic tubes (m-SWCNT) exhibit broad Breit−Wigner−Fano (BWF) line shapes for G−, whereas G+ peaks exhibit Lorentzian shapes.[45] It has been shown that s-SWCNTs exhibit four peaks in this region, at 1607, 1592, 1569, and 1553 cm^{-1}, whereas the spectrum for m-SWCNTs can be fit to a single Lorentzian curve at ~1580 cm^{-1} and a BWF feature in the region ~1530−1560 cm^{-1}. Figure 6 shows Raman G-band spectra at the excitation energy of 1.96 eV for SWCNT films fabricated on several substrates after heating at 130 °C, followed by cooling. In our study, a strong PET peak overlapped with the G+ band and was unchanged by thermal stability tests. However, the G-band frequencies for SWCNT films on bare PET increased by 1−2 cm^{-1} after heating at 130 °C then cooling, even if heating lasted only 10 min, whereas the G-band frequencies for SWCNT films on hard-coated PET and glass substrates were unchanged. These results indicated that the CTE mismatch between SWCNT films and substrates produced compressive stresses on the SWCNTs.[46−48] Armchair tubes can only contribute to the metallic Raman spectra; thus, the peaks at 1582.3 cm^{-1} (metallic G+) were probably dominated by higher symmetry armchair tubes, which improved identification of the strain-induced shifts in the G-band. Moreover, as shown in Figure 6, the G-bands with tangential optical (TO) modes corresponding to atomic displacements along the circumferential direction were more sensitive to stress than G+ bands with longitudinal optical (LO) modes corresponding to atomic displacements along the tube axis, implying that compressive stresses dominated the circumference of the tube due to the uniaxial nanotube structure and the random network structure of the film. The observed upshift in ω_{G+} corresponds to a compressive strain of ~0.1% (assuming the zero-strain ω_{G+} to be 1582.3 cm^{-1}).

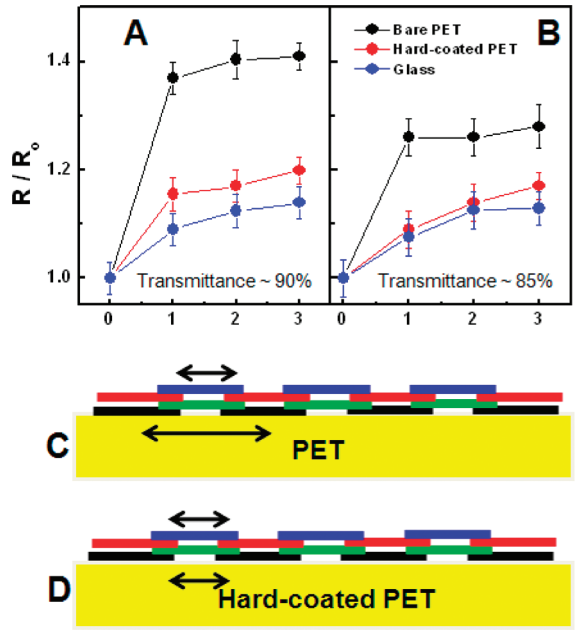

Figure 5. (A and B) Substrate effects on the sheet resistance changes of SWCNT films having different transmittance values, after heating at 130 °C, as a function of the thermal treatment time. Panels C and D show schematic diagram of expansion behavior of SWCNT layers deposited on PET and hard-coated PET after heating.

As shown in Figure 5C,D, the SWCNT network formed a simplified layered structure under the spraying application. The black layer directly interacted with

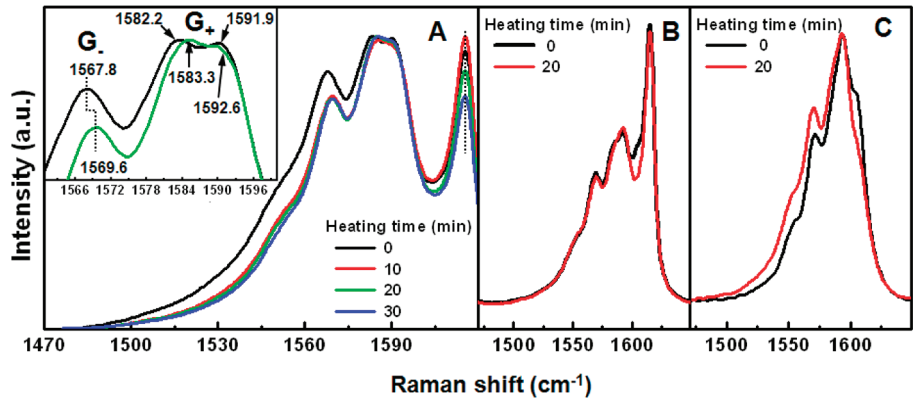

Figure 6. Raman G-band spectra of SWCNT films deposited on (A) bare PET, (B) hard-coated PET, and (C) glass after heating at 130 °C followed by cooling.

the substrate *via* van der Waals forces, which were influenced by the surface or bulk properties of the substrate. However, the top layer was relatively unaffected by the substrate, implying that the substrate-induced strain depended on the film thickness. The reduction in sheet resistance changes for SWCNT films with 85% transmittance, relative to sheet resistance change in films with 90% transmittance, as shown in Figure 5B, may have resulted from the more effective application of compressive strain to thinner SWCNT films. This interpretation was supported by the observation that no Raman band shifts were observed for SWCNT films with 70% transmittance, implying that most SWCNTs were unaffected by the compressive strain induced by the CTE mismatch between SWCNTs and PET.

CONCLUSIONS

We have demonstrated that the surface tension in top coating materials used to passivate bare SWCNT films is crucial for modulating the electrical conductivity of the films. We coated bare SWCNT films with silane sols with different surface tensions, specifically TEOS and MTMS sols. Significantly, top coatings with the TEOS sol, which displayed a high surface tension, unexpectedly reduced the sheet resistance of the film despite the insulating characteristics of SiO_2 due to the nonwetting properties of the TEOS sol on hydrophobic nanotube surfaces. In contrast, the MTMS sol increased the sheet resistance. These different sheet resistance effects were reduced by increasing the surface tension of the SWCNT film *via* gold ion doping. Furthermore, it was demonstrated that the thermal stability of such films on plastic substrates depended on the difference in CTE values of the substrate and SWCNT film. Substrates with small CTEs, such as hard-coated PET and glass, were good substrates for thermally reliable transparent conducting SWCNT films. Analysis of the G-band Raman spectra demonstrated that the CTE mismatch induced compressive strain in the SWNTs after heating followed by cooling. This study characterized previously uninvestigated parameters that contribute to high conductivity and thermal stability in SWCNT-based TCFs on flexible substrates for practical applications.

METHODS

SWCNTs produced by the arc-discharge method and purified by thermal treatment (purchased from Hanwha Nanotech, Inc., AST) were used in this study. SWCNTs were dispersed by bath sonication for 30 min and horn sonication for 1 h in a 1 wt % NaDDBS solution to a concentration of 1 g/L, followed by two rounds of centrifugation at 10 000 rpm for 60 min. The supernatant solution was deposited onto selected substrates using an automatic spray coater (NCS-400) with a 1.2 mm nozzle diameter. The surfactant was removed by dipping in deionized water twice for 10 min each, followed by air drying at 70 °C for 10 min. The substrates used in this study were bare polyethylene terephthalate (PET), hard-coated PET, and glass modified with PTMS for effective adhesion of the SWCNTs. The doping and surface energy modifications of the SWCNT films were achieved by spraying a 0.2 wt % gold(III) chloride solution in ethanol. TEOS and MTMS were purchased from Aldrich and used as precursors for the top coating materials. The silane sols were prepared as follows. Typically, a TEOS sol was prepared by mixing 5 g of TEOS, 2 g of water, 50 mL of ethanol, and 100 μL of 12.1 M HCl, and a continuous sol−gel reaction of it at 60 °C. Water was removed from the prepared sol and the solvent was exchanged with dimethylformamide in a rotary evaporator under vacuum. Other silane sols were prepared by the same method.

Images of the resulting films were obtained by scanning electron microscopy (SEM, HITACHI S4800). Sheet resistance measurements were collected using a four probe tester (Loresta, MCP-T610). The transmittance of each film was measured using a Varian Cary winRV spectrometer. The Raman spectra were measured to characterize the electronic structure of the film at room temperature using a high-resolution Raman spectrometer (LabRAM HR800 UV) with an excitation wavelengths λ of 633 nm. The Raman spectra were obtained by averaging spectra collected from five points on each sample to minimize errors in the data.

Acknowledgment. This work was supported by a grant from the Fundamental R&D Program for Core Technology of Materials funded by the Ministry of Knowledge Economy, and from KERI (Grant No. 10-12-N0101-17), Republic of Korea.

REFERENCES AND NOTES

1. Wu, Z. C.; Chen, Z.; Du, X.; Logan, J. M.; Sippel, J.; Nikolou, M.; Kamaras, K.; Reynolds, J. R.; Tanner, D. B.; Hebard, A. F.;

et al. Transparent, Conductive Carbon Nanotube Films. *Science* **2004**, *305*, 1273–1276.
2. Zhang, M.; Fang, S.; Zakhidov, A. A.; Lee, S. B.; Aliev, A. E.; Williams, C. D.; Atkinson, K. R.; Baughman, R. H. Strong, Transparent, Multifunctional, Carbon Nanotube Sheets. *Science* **2005**, *309*, 1215–1219.
3. Hu, L.; Hecht, D. S.; Grüner, G. Percolation in Transparent and Conducting Carbon Nanotube Networks. *Nano Lett.* **2004**, *4*, 2513–2517.
4. Kaempgen, M.; Duesberg, G. S.; Roth, S. Transparent Carbon Nanotube Coatings. *Appl. Surf. Sci.* **2005**, *252*, 425–429.
5. Parekh, B. B.; Fanchini, G.; Eda, G.; Chhowalla, M. Improved Conductivity of Transparent Single-Wall Carbon Nanotube Thin Films *via Stable Postdeposition Functionalization*. *Appl. Phys. Lett.* **2007**, *90*, 121913/1–121913/3.
6. Zhou, Y.; Hu, L.; Grüner, G. A Method of Printing Carbon Nanotube Thin Films. *Appl. Phys. Lett.* **2006**, *88*, 123109/1–123109/3.
7. Ma, W.; Song, L.; Yang, R.; Zhang, T.; Zhao, Y.; Sun, L.; Ren, Y.; Liu, D.; Liu, L.; Shen, J. Directly Synthesized Strong, Highly Conducting, Transparent Single-Walled Carbon Nanotube Films. *Nano Lett.* **2007**, *7*, 2307–2311.
8. Dan, B.; Irvin, G. C.; Pasquali, M. Continuous and Scalable Fabrication of Transparent Conducting Carbon Nanotube Films. *ACS Nano* **2009**, *3*, 835–843.
9. Tenent, R. C.; Barnes, T. M.; Bergeson, J. D.; Ferguson, A. J.; To, B.; Gedvilas, L. M.; Heben, M. J.; Blackburn, J. L. Ultrasmooth, Large-Area, High-Uniformity, Conductive Transparent Single-Walled-Carbon-Nanotube Films for Photovoltaics Produced by Ultrasonic Spraying. *Adv. Mater.* **2009**, *21*, 3210–3216.
10. Wang, Y.; Di, C.; Liu, Y.; Kajiura, H.; Ye, S.; Cao, L.; Wei, D.; Zhang, H.; Li, Y.; Noda, K. Optimizing Single-Walled Carbon Nanotube Films for Applications in Electroluminescent Devices. *Adv. Mater.* **2008**, *20*, 4442–4449.
11. Geng, H. Z.; Kim, K. K.; Lee, K.; Kim, G. Y.; Choi, H. K.; Lee, S. D.; An, K. Y.; Lee, Y. H. Dependence of Material Quality on Performance of Flexible Transparent Conducting Films With Single-walled Carbon Nanotubes. *NANO* **2007**, *2*, 157–167.
12. Blackburn, J. L.; barnes, T. M.; Beard, M. C.; Kim, Y. -H.; Tenent, R. C.; McDonald, T. J.; To, B.; Coutts, T. J.; Heben, M. J. Transparent Conductive Single-walled Carbon Nanotube Networks with Precisely Tunable Ratios of Semiconducting and Metallic Nanotubes. *ACS Nano* **2008**, *2*, 1266–1274.
13. Geng, J.; Kong, B. -S.; Yang, S. B.; Youn, S. C.; Park, S.; Joo, T.; Jung, H. -T. Effect of SWNT Defects on the Electron Transfer Properties in P3HT/SWNT Hybrid Materials. *Adv. Funct. Mater.* **2008**, *18*, 2659–2665.
14. Kim, K. K.; Bae, J. J.; Park, H. K.; Kim, S. M.; Geng, H. -Z.; Park, K. A.; Shin, H. -J.; Yoon, S. -M.; Benaya, A.; Choi, J. -Y.; et al. Fermi Level Engineering of Single-Walled Carbon Nanotubes by $AuCl_3$ Doping. *J. Am. Chem. Soc.* **2008**, *130*, 12757–12761.
15. Lyons, P. E.; De, S.; Blighe, F.; Nicolosi, V.; Pereira, L. F. C.; Ferreira, M. S.; Coleman, J. N. The Relationship Between Network Morphology and Conductivity in Nanotube Films. *J. Appl. Phys.* **2008**, *104*, 044302/1−044302/8.
16. Hecht, D.; Hu, L. B.; Gruner, G. Conductivity Scaling with Bundle Length and Diameter in Single Walled Carbon Nanotube Networks. *Appl. Phys. Lett.* **2006**, *89* (13), 13112/1–13112/3.
17. Simien, D.; Fagan, J. A.; Luo, W.; Douglas, J. F.; Migler, K.; Obrzut, J. Influence of Nanotube Length on the Optical and Conductivity Properties of Thin Single-Wall Carbon Nanotube Networks. *ACS Nano* **2008**, *2*, 1879–1884.
18. Nirmalraj, P. N.; Lyons, P. E.; De, S.; Coleman, J. N.; Boland, J. J. Electrical Connectivity in Single-Walled Carbon Nanotube Networks. *Nano Lett.* **2009**, *9*, 3890–3895.
19. Geng, H. Z.; Kim, K. K.; So, K. P.; Lee, Y. S.; Chang, Y.; Lee, Y. H. Effect of Acid Treatment on Carbon Nanotube-Based Flexible Transparent Conducting Films. *J. Am. Chem. Soc.* **2007**, *129*, 7758–7759.
20. Zahab, A.; Spina, L.; Poncharal, P. Water-Vapor Effect on the Electrical Conductivity of a Single-Walled Carbon Nanotube mat. *Phys. Rev. B* **2000**, *62*, 10000–10003.
21. Pati, R.; Zhang, Y.; Nayaka, S. K.; Ajayan, P. M. Effect of H_2O Adsorption on Electron Transport in a Carbon Nanotube. *App. Phys. Lett.* **2002**, *81*, 2638–2640.
22. Jackson, R.; Domercq, B.; Jain, R.; Kippelen, B.; Graham, S. Stability of Doped Transparent Carbon Nanotube Electrodes. *Adv. Funct. Mater.* **2008**, *18*, 2548–2554.
23. Wang, G. F.; Tao, X. M.; Wang, R. X. Flexible Organic Light-Emitting Diodes with a Polymeric Nanocomposite Anode. *Nanotechnology* **2008**, *19*, 145201–145205.
24. Wood, J. R.; Frogley, M. D.; Meurs, E. R.; Prins, A. D.; Peijs, T.; Dunstan, D. J.; Wagner, H. D. Mechanical Response of Carbon Nanotubes under Molecular and Macroscopic Pressures. *J. Phys. Chem. B* **1999**, *103*, 10388–10392.
25. Ozel, T.; Abdula, D.; Hwang, E.; Shim, M. Nonuniform Compressive Strain in Horizontally Aligned Single-Walled Carbon Nanotubes Grown on Single Crystal Quartz. *ACS Nano* **2009**, *3*, 2217–2224.
26. Heyd, R.; Charlier, A.; McRae, E. Uniaxial-Stress Effects on the Electronic Properties of Carbon Nanotubes. *Phys. Rev. B* **1997**, *55*, 6820–6824.
27. Yang, L; Anantram, M. P.; Han, J.; Lu, J. P. Band-Gap Change of Carbon Nanotubes: Effect of Small Uniaxial and Torsional Strain. *Phys. Rev. B* **1999**, *60*, 13874–13878.
28. Yang, L.; Han, J. Electronic Structure of Deformed Carbon Nanotubes. *Phys. Rev. Lett.* **2000**, *85*, 154–157.
29. Minot, E. D.; Yaish, Y.; Sazonova, V.; Park, J. -Y.; Brink, M.; McEuen, P. L. Tuning Carbon Nanotube Band Gaps with Strain. *Phys. Rev. Lett.* **2003**, *90*, 156401/1–156401/4.
30. Capaz, R. B.; Spararu, C. D.; Tangney, P.; Cohen, M. L.; Loui, S. G. Hydrostatic Pressure Effects on the Structural and Electronic Properties of Carbon Nanotubes. *Phys. Status Solidi B* **2004**, *14*, 3352–3359.
31. Filho, A. G. S.; Kobayashi, N.; Jiang, J.; Grüneis, A.; Saito, R.; Cronin, S. B.; Filho, J. M.; Samsonidze, Ge., G.; Dresselhaus, G.; Dresselhaus, M. S. Strain-Induced Interference Effects on the Resonance Raman Cross Section of Carbon Nanotubes. *Phys. Rev. Lett.* **2005**, *95*, 217403/1–217403/4.
32. Doherty, E. M.; De, S.; Lyons, L.; Shmelov, A.; Nirmalraj, P. N.; Scardaci, V.; Blau, W. J.; Boland, J. J.; Coleman, J. N. The Spatial Uniformity and Electromechanical Stability of Transparent, Conductive Films of Single Walled Nanotubes. *Carbon* **2009**, *47* (10), 2466–2473.
33. Geng, H. Z.; Lee, D. S.; Kim, K. K.; Han, G. H.; Park, H. K.; Lee, Y. H. Absorption Spectroscopy of Surfactant-Dispersed Carbon Nanotube Film: Modulation of Electronic Structures. *Chem. Phys. Lett.* **2008**, *455* (4−6), 275–278.
34. Kinloch, A. J. *Adhesion and Adhesives Science and Technology*; Chapman and Hall Ltd.: London, 1987; pp 82.
35. Wu, S. *Polymer Interface and Adhesion*; Marcel Dekker, Inc.: New York, 1982; pp 106−112.
36. Han, J. T.; Kim, S. Y.; Jeong, H. J.; Jeong, S. Y.; Lee, G. -W. Molecular Engineering to Minimize the Sheet Resistance Increase of Single-Walled Carbon Nanotube/Binder Hybrid Conductive Thin Films. *J. Phys. Chem. C* **2009**, *113*, 16915–16920.
37. De, S.; Lyons, P. E.; Sorel, S.; Doherty, E. M.; King, P. J.; Blau, W. J.; Nirmalraj, P. N.; Boland, J. J.; Scardaci, V.; Joimel, J.; et al. Transparent, Flexible, and Highly Conductive Thin Films Base on Polymer-Nanotube Composites. *ACS Nano* **2009**, *3*, 714–720.
38. Dujardin, E.; Ebbesen, T. W.; Hiura, H.; Tanigaki, K. Capillarity and Wetting of Carbon Nanotubes. *Science* **1994**, *265*, 1850–1852.
39. Dujardin, E.; Ebbesen, T. W.; Krishnan, A.; Treacy, M. M. J. Wetting of Single Shell Carbon Nanotubes. *Adv. Mater.* **1998**, *10*, 1472–1475.
40. Tillman, N.; Ulman, A.; Schildkraut, J. S.; Penner, T. L. Incorporation of Phenoxy Groups in Self-Assembled Monolayers of Trichlorosilane Derivatives: Effects on Film Thickness, Wettability, and Molecular Orientation. *J. Am. Chem. Soc.* **1998**, *111*, 6136–6144.
41. Ulatowska-jara, A.; Hołowacz, I.; Wysocka, K.; Podbielska, H.

Silica-Based Versus Silica-Titania Sol-Gel Materials-Comparison of the Physical Properties: Surface tension, Gelation time, Refractive Index and Optical Transmittance. *Optica Appl.* **2009**, *XXXIX*, 211–220.
42. Jiang, H.; Liu, B.; Huang, Y.; Hwang, K. C. Thermal Expansion of Single Wall Carbon Nanotubes. *J. Eng. Mater. Technol.* **2004**, *126*, 265–270.
43. Li, H. D.; Yue, K. T.; Lian, Z. L.; Zhan, Y.; Zhou, L. X.; Zhang, S. L.; Shi, Z. J.; Gu, Z. N.; Liu, B. B.; Yang, R. S.; et al. Temperature Dependence of the Raman Spectra of Single-Wall Carbon Nanotubes. *Appl. Phys. Lett.* **2000**, *76*, 2053–2055.
44. Ni, Z. H.; Yu, T.; Lu, Y. H.; Wang, Y. Y.; Feng, Y. P.; Shen, Z. X. Uniaxial Strain on Graphene: Raman Spectroscopy Study and Band-Gap Opening. *ACS Nano* **2008**, *2*, 2301–2305.
45. Frogley, M.; Zhao, Q.; Wagner, H. Polarized Resonance Raman Spectroscopy of Single-Wall Carbon Nanotubes within a Polymer Under Strain. *Phys. Rev. B* **2002**, *65*, 113413/1–113413/4.
46. Venkateswaran, U. D.; Rao, A. M.; Richter, E.; Menon, M.; Rinzler, A.; Smalley, R. E.; Eklund, P. C. Probing the Single-Wall Carbon Nanotube Bundle: Raman Scattering under High Pressure. *Phys. Rev. B* **1999**, *59*, 10928–10934.
47. Amer, M. S.; El-Ashry, M. M.; Maguire, J. F. Study of the Hydrostatic Pressure Dependence of the Raman Spectrum of Single-Walled Carbon Nanotubes and Nanospheres. *J. Chem. Phys.* **2004**, *121*, 2752–2757.
48. Lebedkin, S.; Arnold, K.; Kiowski, O.; Hennrich, F.; Kappes, M. M. Raman Study of Individually Dispersed Single-Walled Carbon Nanotubes Under Pressure. *Phys. Rev. B* **2006**, *73*, 094109.